Pore Wall of a Mesoporous Molecular Sieve Derived from Kanemite

S. Inagaki,*,† Y. Sakamoto,‡ Y. Fukushima,† and O. Terasaki*,‡

Toyota Central R&D Labs., Inc., 41-1, Yokomichi Nagakute, Aichi, 480-11, Japan, and Department of Physics, Graduate School of Science and Center for Interdisciplinary Research, Tohoku University, Sendai, 980-77, Japan

Received February 9, 1996. Revised Manuscript Received June 19, 1996[⊗]

The pore diameters and pore wall thicknesses of the mesoporous molecular sieves FSM-16 derived from a layered silicate (kanemite) were estimated by X-ray diffraction, physisorption, transmission electron micrographs, ^{29}Si MAS NMR, and modeling and simulation. The XRD simulation with a simple model of a hexagonal array of cylinders gave reasonable values coinciding with those obtained by TEM and nitrogen adsorption, with some corrections. As-synthesized FSM-16 material had pore walls 0.4 nm thick, corresponding to the slightly less wrinkled single SiO_4 tetrahedral layer observed in the crystalline layered silicate minerals, and an apparent pore diameter of 4.2 nm. Surfactant-free FSM-16, formed by calcination and exchange for H^+, had thicker pore walls of 0.8 and 0.9 nm corresponding to double SiO_4 tetrahedral layers and pore diameters of 3.4 and 3.7 nm.

Introduction

A new family of mesoporous molecular sieves with hexagonal and cubic symmetry has been synthesized. This is expected to be used as excellent catalysts and absorbents for relatively large size molecules. MCM-41[1,2] and FSM-16[3,4] materials are members of this family, both with a hexagonal arrangement of cylindrical nanopores, which have been synthesized from aluminosilicate gels and layered silicate kanemite respectively, using surfactants. Their pore walls are considered to be amorphous rather than crystalline,[2,5] so pore diameters cannot be determined from their crystallographic data. Although physisorption of nitrogen[5−8] and argon[2] or transmission electron micrographic observation[2,5,7] have been used to estimate the pore diameters or wall thicknesses, they have some weaknesses for determining the precise dimensions. The modeling of the MCM-41 structure and calculation of their X-ray diffraction patterns have been tried to determine the pore diameters and wall thicknesses. Beck et al.[2] reported that the MCM-41 models with a hexagonal array of cylinders whose walls were composed of both a zeolitic and continuous shell-like structure gave similar diffraction patterns containing four or five peaks in the low-angle region. They concluded that diffraction intensities were of limited use in determining the pore wall structure for the mesoporous materials. Stucky et al.[9] estimated the pore wall thickness of MCM-41 at 0.8 (±0.1) nm by fitting X-ray experimental data to a model of a hexagonal array of void tubes which assumed an amorphous continuous scatter for the tube walls. They have proposed that the pore wall structure was made up of two silicate monolayers because of the estimated dimension of the pore wall. Feuston et al.[10] carried out molecular dynamics simulations of models for the MCM-41 materials with various wall thicknesses and compared the calculated and experimental X-ray diffraction patterns. The model structure amorphous silica wall with >1.0 nm thickness was in agreement with that observed experimentally. But, these examinations are not definitive to determine the pore diameters and wall thickness of the mesoporous materials. It is necessary to determine the pore diameter and wall thickness more precisely by combining various measurements and simulations.

It has yet been clarified whether the pore-wall structures of the MCM-41 and FSM-16 materials are the same or different. Their thermal stability[7] and adsorption properties[11] have been reported to be somewhat different. The pore-wall structure such as pore-wall thickness and surface structure are important factors to determine the thermal stability and catalytic and adsorption properties of the mesoporous molecular sieves.

Here we try to determine the pore diameter and pore-wall thickness of the FSM-16 materials by X-ray dif-

† Toyota Central R&D Labs.

‡ Tohoku University.

[⊗] Abstract published in *Advance ACS Abstracts,* August 15, 1996.

(1) Kresge, C. T.; Leonowicz, M. E.; Roth, W. J.; Vartuli, J. C.; Beck, J. S. *Nature* **1992**, *359*, 710−712.

(2) Beck, J. S.; Vartuli, J. C.; Roth, W. J.; Leonowicz, M. E.; Kresge, C. T.; Schmitt, K. D.; Chu, C. T.-W.; Olson, D. H.; Sheppard, E. W.; McCullen, S. B.; Higgins, J. B.; Schlenker, J. L. *J. Am. Chem. Soc.* **1992**, *114*, 10834−10843.

(3) Inagaki, S.; Fukushima, Y.; Kuroda, K. *J. Chem. Soc., Chem. Commun.* **1993**, 680−682.

(4) Inagaki, S.; Koiwai, A.; Suzuki, N.; Fukushima, Y.; Kuroda, K. *Bull. Chem. Soc., Jpn.* **1996**, *69*, 1449−1457.

(5) Chen, C.-Y.; Li, H.-X.; Davic, M. E. *Microporous Mater.* **1993**, *2*, 17−26.

(6) Branton, P. J.; Hall, P. G.; Sing, K. S. W.; Reichert, H. R.; Schuth, F.; Unger, K. K. *J. Chem. Soc., Faraday Trans.* **1994**, *90*, 2965−2967.

(7) Chen, C.-Y.; Xiao, S.-Q.; Davis, M. E. *Microporous Mater.* **1995**, *4*, 1−20.

(8) Schmidt, R.; Hansen, E. W.; Stocker, M.; Akporiaye, D.; Ellestad, O. H. *J. Am. Chem. Soc.* **1995**, *117*, 4049−4056.

(9) Stucky, G. D.; Monnier, A.; Schuth, F.; Huo, Q.; Margolese, D.; Kumar, D.; Krishnamurty, M.; Petroff, P.; Firouzi, A.; Janicke, M.; Chmelka, B. F. *Mol. Cryst. Liq. Cryst.* **1994**, *240*, 187−200.

(10) Feuston, B. P.; Higgins, J. B. *J. Phys. Chem.* **1994**, *98*, 4459−4462.

(11) Inagaki, S.; Fukushima, Y.; Kuroda, K.; Kuroda, K. *J. Colloid Interface Sci.* **1996**, *180*, 623−624.

S0897-4756(96)00115-9 CCC: $12.00

fraction, physisorption, transmission electron micrograph, ^{29}Si MAS NMR, and modeling and simulations.

Experimental Section

Preparation of Samples. A spray-dried sodium silicate water-glass powder, whose SiO_2/Na_2O ratio was adjusted to 2.00, was supplied by Nippon Kagaku Kogyo Corp. Hexadecyltrimethylammonium [HDTMA, $C_{16}H_{33}N^+(CH_3)_3$] chloride were obtained from Tokyo Kasei and used without further purification.

δ-$Na_2Si_2O_5$ was obtained after calcination of the sodium silicate powder at 700 °C for 6 h. δ-$Na_2Si_2O_5$ powder (50 g) was dispersed in 500 cm^3 of distilled water and stirred for 3 h at room temperature. Filtration of the dispersion gave a wet kanemite paste. X-ray powder diffraction of the dried sample confirmed the formation of kanemite.

The wet kanemite was dispersed in a 1000 cm^3 of a 0.1 mol dm^{-3} HDTMA chloride solution. The pH of the suspension was 12.3. After heat treatment of the suspensions at 70 °C for 3 h, the pH of the dispersion was adjusted to 8.5 by addition of a 2 mol dm^{-3} HCl aqueous solution. The suspensions were heated further for 3 h and then cooled to room temperature. Filtered solid products were washed five times with 1000 cm^3 distilled water and dried at 50 °C. This as-synthesized FSM-16 material is called HDTMA/FSM-16. Although some fraction of kanemite dissolved during the synthesis in pH = 12.3, FSM-16 material was formed from the silicate sheets of kanemite.[4] The surfactants in the as-synthesized materials have been removed by two different kinds of treatments, that is, calcination and treatment with ethanol solution with HCl. The as-synthesized material was calcined at 550 °C for 6 h in air, and the calcined sample was called FSM-16. One gram of the as-synthesized material was dispersed in 150 cm^3 of ethanol with 3.8 g of 36 wt % chloric acid aqueous solution. After keeping the dispersion at 50 °C for 6 h under stirring, the product was recovered by filtration. This treatment with ethanol solution was repeated twice. The sample was called H/FSM-16. A diffuse reflection Fourier transform infrared spectroscopy of the H/FSM-16 sample did not show reflection peaks due to HDTMA, indicating complete removal of surfactants for the H/FSM-16 sample.

Characterization. X-ray powder diffraction (XRD) patterns of the HDTMA/FSM-16, H/FSM-16, and FSM-16 samples were obtained by using a Philips X'Pert-MPD diffractometer with Cu Kα radiation. The intensity profiles were measured in each step for 10 s and step width of 0.040 in 2θ with divergent slits of $^1/_{16}$. To measure the effective "lattice constant", Si powder was used as an internal standard. XRD patterns of H/FSM-16 and the treated sample with water vapor were also obtained by a Rigaku RAD-B diffractometer with Cu Kα radiation. The water vapor of $P/P_0 = 0.9$ was exposed on H/FSM-16 at 25 °C in a vacuum system. The diffraction patterns were measured by a continuous scan rated at 1°/min, and slits of 0.5°−0.15 mm−0.5°. Solid-state ^{29}Si MAS NMR spectra were recorded on a Bruker MSL-300WB spectrometer at 59.620 MHz spinning 4 kHz using pulses at 90-s intervals. A peak intensity was not changed when the pulse intervals was over 90 s. N_2 adsorption isotherms at −196 °C were measured by means of a volumetrical method using a conventional vacuum line with a Baratron pressure transducer (127AA) and controlled valves (248A). Pore diameters were calculated by a corrected Kelvin equation in which a multilayer adsorption was taken into consideration. The kelvin equation gives a pore dimameter assuming a cylindical pore. The surface tension and molar volume of nitrogen which are included by the Kelvin equation are taken to be the values of liquid nitrogen at 77 K. The thickness of the multilayer adsorption was estimated from adsorption data of nitrogen on nonporous silica reported by Bhambhani et al.[12] Specific surface areas were calculated by the BET method using the adsorption data collected from $P/P_0 = 0.05$ to P/P_0 just below the capillary condensation. The pore volumes were obtained from the saturated adsorption amount of nitrogen by assuming that the pore was filled with condensed liquid nitrogen. Transmission electron micrographs (TEM) were recorded with a JEOL JEM-200CX at an accelerating voltage of 200 kV. The HDTMA/FSM-16 sample was observed directly on a Cu mesh by TEM. The FSM-16 sample was buried in epoxy resins and sectioned for TEM observation.

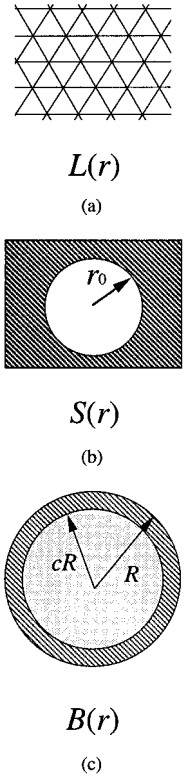

Figure 1. Schematic drawings of a lattice function $L(r)$ (a), a size function $S(r)$ (b), and a basis function $B(r)$ (c).

Model and Simulations. We can describe a crystal of a certain size $C(r)$, in terms of convolution of a lattice function, $L(r)$, multiplied by a size function, $S(r)$, with a basis function, $B(r)$:

$$C(r) = \{L(r)\cdot S(r)\}*B(r) \quad (1)$$

where the vector r is a general position vector in crystal and * shows an operation of convolution, as schematically shown in Figure 1. The intensity of X-ray diffraction (XRD), I, is given by the square of the crystal structure factor, which is the Fourier transform, **F**, of $C(r)$:

$$I \propto [\mathbf{F}[\{L(r)\cdot S(r)\}*B(r)]]^2 = [\mathbf{F}\{L(r)\}*\mathbf{F}\{S(r)\}\cdot\mathbf{F}\{B(r)\}]^2 \quad (2)$$

We observed four peaks in an XRD pattern of FSM-16, and their positions could be indexed by a hexagonal lattice. We could not observe any reflections with $hkil$, $l \neq 0$, in either XRD patterns or electron diffraction (ED) patterns, and any deviations from hexagonal symmetry in ED patterns. Therefore it is reasonable to assume that the lattice $L(r)$ is taken to be hexagonal and that the basis is uniform along the z direction.

Since TEM images indicate that the size of FSM-16 "crystallite" does not show anisotropy in terms of the structure perpendicular to the z axis, it is reasonable to assume that the shape of the size function is considered as circle. Therefore if the size, r_0, of the size function is decided, the size function $S(r)$ is given by

(12) Bhambhani, M. R.; Cutting, P. A.; Sing, K. S. W.; Turk, D. H. *J. Colloid Interface Sci.* **1972**, *38*, 109−117.

$$S(r) = 1 \quad \text{for } r \le r_0$$
$$= 0 \quad \text{for } r \ge r_0 \tag{3}$$

To solve the structure, in this case, the structure of the basis, we must first determine the effects from the lattice and the size and derive the structure factors for four peaks from the observation. We can obtain absolute values of the structure factors for these, but to obtain $B(r)$ by Fourier synthesis, we must assume relative phase relations among the reflections.

There are two contributions to randomness, one is within a crystallite and the other is some kind of distribution among the crystallites. ED patterns can be obtained from specimens of smaller area than XRD, still we cannot observe higher order reflections. XRD gives average information over the crystallites in the X-ray beam.

Many papers have dealt with the XRD patterns of MCM-41 and several functions for the basis have been assumed. Two extremes are cylindrical and hexagonal geometries. Both cylindrical and hexagonal models give fairly good correspondence with the experimentally obtained XRD patterns. We may conclude, in short, that the detail of the structure of the basis is hardly determined by only four observed peaks. Therefore in this simulation, by taking into consideration the fact that the basis has pores, which is clear from N_2 adsorption and TEM images, we assumed the cylindrical model with hexagonal symmetry induced by introducing a parameter which indicate relationship of the distance between the neighboring rods. By introducing this parameter, the effect of hexagonal symmetry can be included by allowing an overlap with the nearest-neighbor rods even within a cylindrical model.

To simulate the XRD intensity profiles for HDTMA/FSM-16, H/FSM-16, and FSM-16 samples, we assumed that FSM-16 consists of a hexagonal arrangement of infinitely long cylindrical rods. Following the discussion by Oster et al.,[13] the scattering intensity from these systems was derived. We define the normalized intensity of scattering from the systems composed of n cylinders by the following equation:

$$(1/n^2)\, F^2(kR) \sum_p^n \sum_q^n J_0(ks_{pq}) \tag{4}$$

where s_{pq} is the distance between the centers of the pth and qth cylinder and k is scattering vector defined by $k = (4\pi/\lambda)\sin\theta$. $F(kR)$ is the scattering factor from an isolated infinitely long cylindrical rod. Parameter n is the number of cylinders inside of the circle, $r \le r_0$, determined in eq 3. To extend this treatment to the problem for tube shape, we introduced a parameter c so that the thickness of the tube is given by $(1 - c)R$, $1 > c > 0$. Then $F(kR)$ is explicitly given for an isolated infinitely long cylindrical tube:

$$F(kR) = 2\left[\frac{J_1(kR) - cJ_1(ckR)}{kR(1 - c^2)}\right] \tag{5}$$

where $J_1(kr)$ is the first-order cylindrical Bessel function and R is the radius of the cylinder.

For a system with seven cylinders, the intensity is written down by introducing a new parameter γ as $2R/s$ in the following:

$$(1/49)F^2(x/2\gamma)[7 + 24J_0(x) + 6J_0(x) + 12J_0(\sqrt{3}x)] \tag{6}$$

where $x = 2\gamma kR = ks$.

Figure 2 shows the dependence of the intensity on the numbers of tubes n. The figure gives the intensity profile for the systems with $n = 7$, 19, 37, and 61. The vertical lines in the figure give the positions of the hexagonal 10, 11, 20, and 21 reflections, respectively. It is clear from the figure that reflection profiles becomes sharper and the positions of the reflections moved towards those expected from the hexagonal lattice, and the intensity decreases, except in the region of $k \sim 0$, as n increases. The dependencies of the intensity profile on the parameters c and γ were examined for the case of $n = 61$. The reason for taking $n = 61$ will be shown later. Figure 3 shows that the relative intensity of the peaks changed systematically with the parameter c, although the positions of the peak do not shift, while the intensity did not change with γ systematically, as shown in Figure 4. Furthermore to calculate the XRD pattern for HDTMA/FSM-16, which has surfactant within each tube, we consider the rod which consists of tubes filled by material with different scattering amplitude from that of the tube (see Figure 1c). We introduced the parameter a defined by the ratio of the scattering amplitudes for the material to the tube and $1 > a > 0$ for our case. For the normalized intensity of scattering by these rods, the scattering amplitudes F of an isolated cylindrical rod is given by

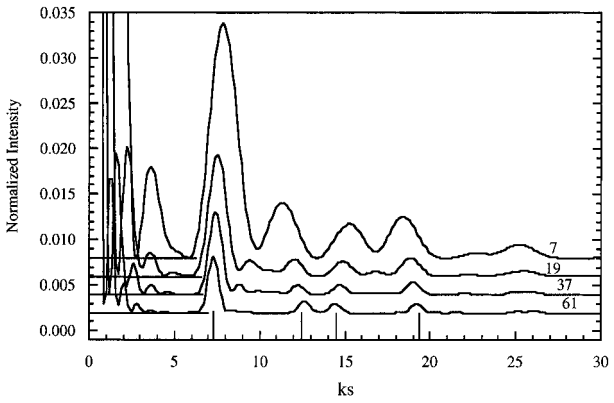

Figure 2. Dependence of the intensity on the numbers of tubes n ($c = 0.65$, $\gamma = 1$). The intensity is unity at $ks = 0$. Four lines indicate the peak positions of the hexagonal lattice.

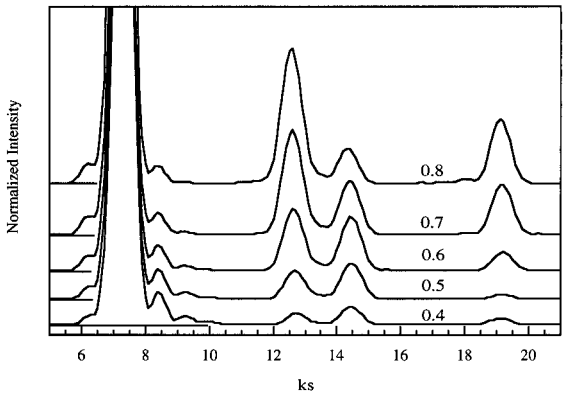

Figure 3. Dependence of the intensity on the parameter c ($n = 61$, $\gamma = 0.8$). The intensity is normalized to the first peak.

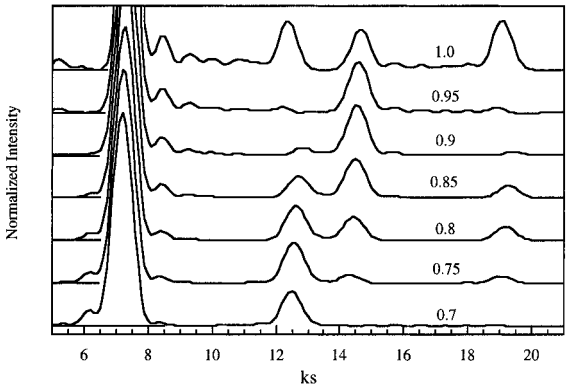

Figure 4. Dependence of the intensity on the parameter $\gamma = 2R/s$ ($n = 61$, $c = 0.65$). The intensity is normalized to the first peak.

(13) Oster; G.; Riley, D. P. *Acta Crystallogr.* **1952**, *5*, 272−276.

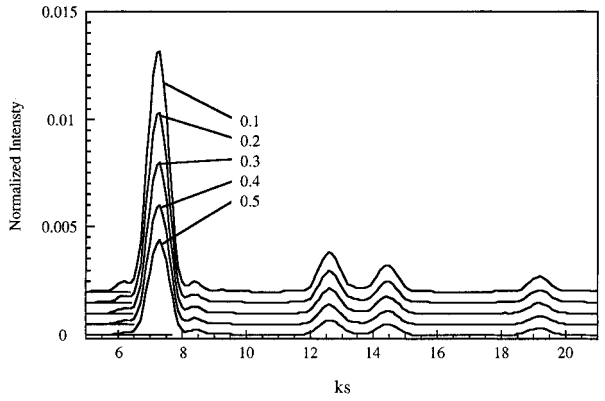

Figure 5. Dependence of the intensity on the parameter a ($n = 61$, $c = 0.65$, $\gamma = 0.8$). The intensity is unity at $ks = 0$.

$$F(kR) = 2\left[\frac{J_1(kR) - (1-a)cJ_1(ckR)}{kR[1-(1-a)c^2]}\right] \qquad (7)$$

By substitution for eq 4, we obtain the intensity profile for the various systems. Figure 5 shows dependence of the intensity on the parameter a. The relative intensity of these four peaks do not change, when a is changed, although the absolute intensity changes very much. Therefore, as far as we discuss only the relative intensity, the XRD patterns is independent of a.

It has been shown that the intensity of an assembly of cylindrical rods is obtained by using four parameters, n, a, c, and γ. Parameter n, which indicates the size of hexagonal lattice, influences the term in the eq 4:

$$(1/n^2)\sum_{p}^{n}\sum_{q}^{n} J_0(ks_{pq}) \qquad (8)$$

This gives the position of the reflections (hexagonal peaks) in 2θ and the width of the peaks. This equation is a function of the product of a lattice function, $L(r)$, and a size function, $S(r)$, in the first discussion. On the other hand the parameters a, c, and γ effect the scattering amplitude F, dependent on the structure of an isolated cylindrical rod, and the basis function, $B(r)$. This term gives the intensity of each peak whose position is given by the eq 5, i.e., parameter n.

To fit the simulated intensity profile to the experimentally obtained XRD pattern, we adjusted four parameters. Actually, in a hexagonal arrangement of more than 37 rods, the peak positions do not change and the case of $n = 61$ gives peak positions close to those observed. We therefore carried out fitting assuming $n = 61$. Furthermore since we confine ourselves to relative intensity, the effect of the parameter a has been ignored even for HDTMA/FSM-16, which contains a template. As mentioned before, absolute intensity is very sensitive to the choice of a, we will treat this in a future publication.

Results

Figure 6 shows the experimental and simulated XRD patterns of HDTMA/FSM-16, H/FSM-16, and FSM-16 samples. We have performed qualitative fittings of the XRD patterns by comparing not the relative integral intensity but the relative intensity of the each peak position, normalized to the first of four peaks and revised in terms of Lorentz polarization factor. Thus, the width of the peak and the background intensity are not considered in this simulation, and the relative intensity of each peak does not fit completely. However, each simulated pattern gives good correspondence with the experimentally obtained XRD pattern. The pore space is not spherical, because of overlap with the nearest neighbor rods. The pore diameters of each simulated model are derived therefore as an effective

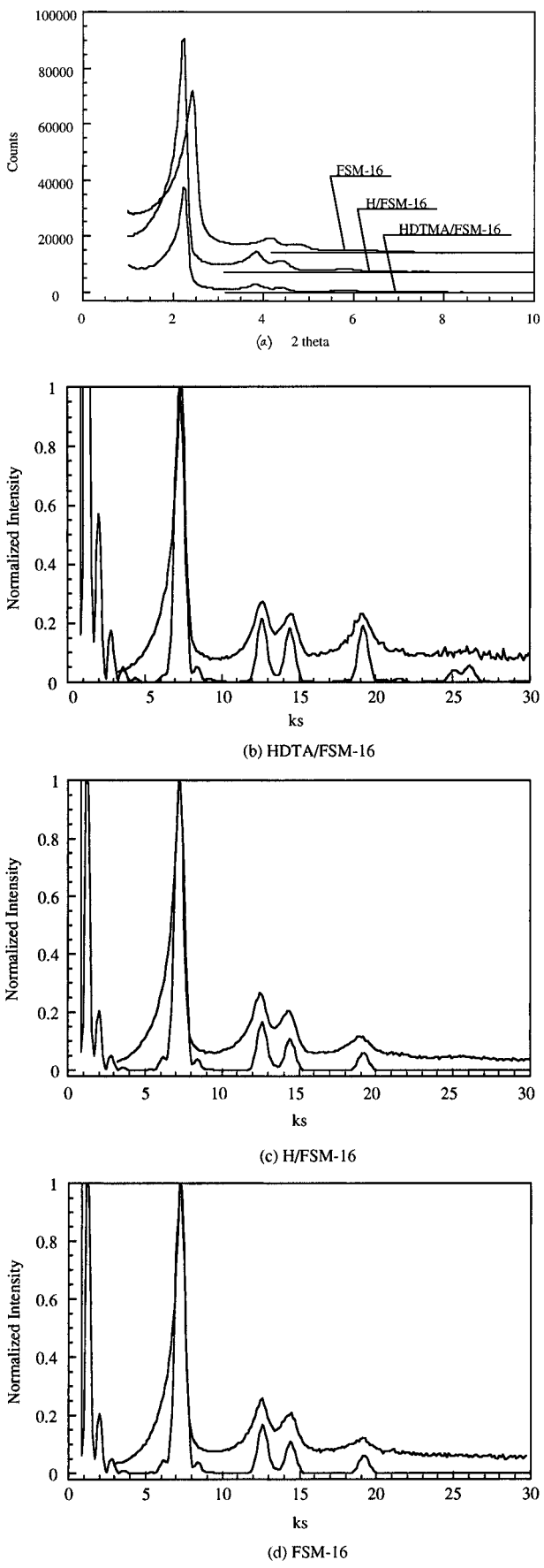

Figure 6. Experimental XRD patterns (a) of HDTMA/FSM-16, H/FSM-16, and FSM-16, and simulated XRD patterns of HDTMA/FSM-16 (b), H/FSM-16 (c), and FSM-16 (d).

Table 1. Pore Diameters (*d*, nm) and Pore-Wall Thicknesses (*t*, nm) Determined by Various Methods

	HDTMA/FSM-16 ($a = 4.61 \pm 0.03$)		H/FSM-16 ($a = 4.59 \pm 0.04$)		FSM-16 ($a = 4.25 \pm 0.04$)	
methods	*d*	*t*	*d*	*t*	*d*	*t*
XRD simulation	4.2	0.4	3.7	0.9	3.4	0.8 (±0.1)
N_2 adsorption			3.1	1.5	2.7	1.6 (±0.1)
TEM	4.1	0.5			3.1	1.2 (±0.2)

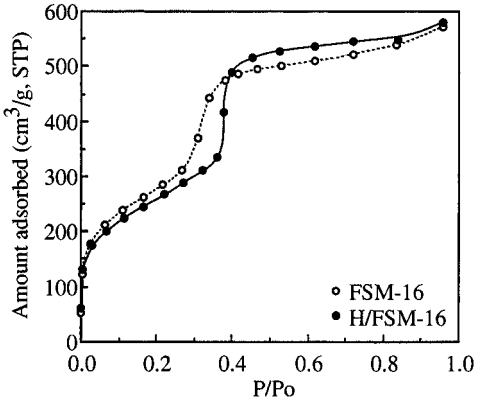

Figure 7. Nitrogen adsorption isotherms for H/FSM-16 and FSM-16.

Table 2. Surface Areas and Pore Volumes Determined from N_2 Adsorption Isotherms

samples	surface area (m^2/g)	pore vol (cm^3/g)
H/FSM-16	911	0.81
FSM-16	990	0.77

pore diameter by assuming that the cross section of the pore space is a circle, and the wall thickness is derived from the eq s-2R as an effective wall thickness, which is equal to the minimum, listed in Table 1. The errors in the XRD simulation are the combined error of the lattice parameter and of the XRD pattern fitting. The former results from the XRD experiments, and the latter from the error of the fitting parameters in which we consider that the simulated patterns are of a similar shape as the observed one.

Figure 7 shows nitrogen adsorption isotherms for the H/FSM-16 and FSM-16 samples. Steep increases in adsorption at around $P/P_0 = 0.3$ are due to nitrogen filling the mesopores. The range of P/P_0 at the steep increases were 0.35−0.41 for H/FSM-16 and 0.28−0.37 for FSM-16, respectively. The narrower range of the P/P_0 values for the former case indicates a less scattered pore size distribution for H/FSM-16 than FSM-16 samples. Pore diameters were calculated from the inflection points on the steep rises of adsorption curves and listed in Table 1. The pore diameter of FSM-16 is smaller than that of H/FSM-16. The pore-wall thicknesses, which were calculated by subtraction of the pore diameters from the unit-cell dimensions determined by XRD are also listed in Table 1. There is no notable difference in wall thickness between H/FSM-16 and FSM-16. The specific surface areas and pore volumes calculated from the adsorption isotherm of nitrogen are listed in Table 2.

Transmission electron micrographs of HDTMA/FSM-16 and FSM-16 samples are shown in Figure 8. They show a regular pore arrangement. It was observed that FSM-16 samples had smaller pore diameter and thicker pore wall than HDTMA/FSM-16. The pore diameters and wall thicknesses estimated from the photographs

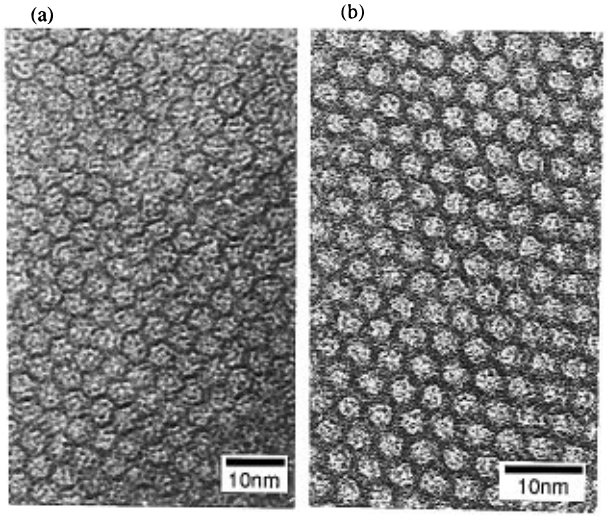

Figure 8. HREM images of (a) HDTMA/FSM-16 and (b) FSM-16.

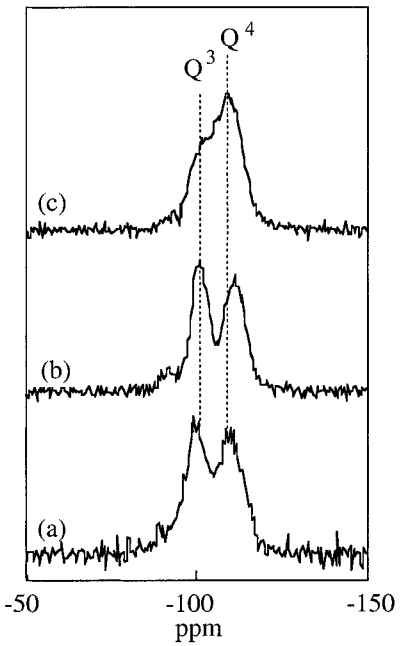

Figure 9. ^{29}Si NMR spectra of (a) HDTMA/FSM-16, (b) H/FSM-16 and (c) FSM-16.

by standardizing the pore intervals equal to unit-cell dimensions are listed in Table 1.

Figure 9 shows ^{29}Si MAS NMR spectra of the three materials. As-synthesized FSM-16 material (HDTMA/FSM-16) had SiO_4 units due to both Q^3 and Q^4 environments with almost the same intensity. H/FSM-16 sample showed a NMR spectrum similar to that of the HDTMA/FSM-16 sample, which suggested that further condensation of SiO_4 tetrahedra in the pore wall had not occurred during the exchange of surfactants for H^+. For the FSM-16 sample a broadened Q^4 signal with a small-shoulder Q^3 signal was observed in the NMR spectrum. Clearly, the SiO_4 tetrahedra condensed

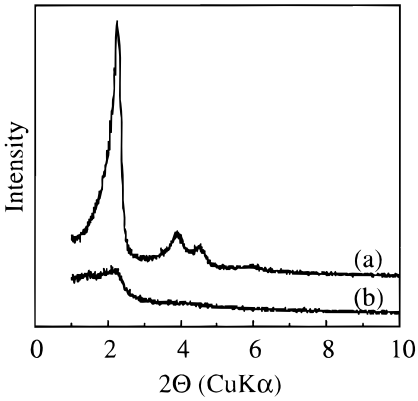

Figure 10. XRD patterns of (a) H/FSM-16 and (b) that treated with water vapor at 25 °C.

further and the structural ordering around SiO_4 tetrahedra decreased during calcination.

XRD patterns shown in Figure 10 show that the regular pore-arranged structure of H/FSM-16 sample disappeared after exposure to water vapor at 25 °C. This indicates that the framework structure of H/FSM-16 sample is unstable. On the other hand, the calcined sample, FSM-16, shows an unchanged XRD pattern even after exposure to water vapor.

Discussion

The pore diameters and pore-wall thicknesses determined by the XRD simulations, nitrogen adsorption isotherms, and transmission electron micrographs are almost coincident with each other, as shown in Table 1. The pore diameters estimated by nitrogen adsorption are smaller than those estimated by the other methods. They are average diameters assuming a cylindical pore. The Kelvin equation does not remain strictly valid for very fine pores below a pore radii of about 50 nm.[14] As the nonnegligible effect of surface potential due to the pore walls is not considered in the Kelvin equation, values for the surface tension and molar volume used in the Kelvin equation are not equal to those of bulk liquid. The surface tension of liquid in a small pore of 2 nm in diameter has been reported to be about 1.5 times larger than the bulk value.[14] Calculations using this corrected surface tension gave pore diameters of 4.0 and 3.5 nm for H/FSM-16 and FSM-16 samples, respectively. Because the molar volume of liquid in a small pore seems to be smaller than the bulk value, the actual pore diameter would be estimated between 3.0 and 4.0 nm for H/FSM-16 and 2.7 and 3.5 nm for FSM-16 samples. Note that these are kinetic diameters of the pores including the effects of vibrating atoms of the pore walls and vibrating nitrogen molecules.

Generally speaking, thicknesses obtained from electron micrographs tend to be larger than actual ones when the axis of the crystal is inclined or the crystal bends with respect to the direction of electron beam. However, the wall thicknesses obtained by TEM are in good agreement with those of the XRD simulations. Chen et al.[7] reported from TEM observations that the wall thickness of a mesoporous material derived from kanemite was 0.8 nm. This value is in good agreement with our result.

(14) Gregg, S. J.; Sing, K. S. W. *Adsorption, Surface Area and Porosity*, 2nd ed.; Academic Press: New York, 1982; pp 153−60.

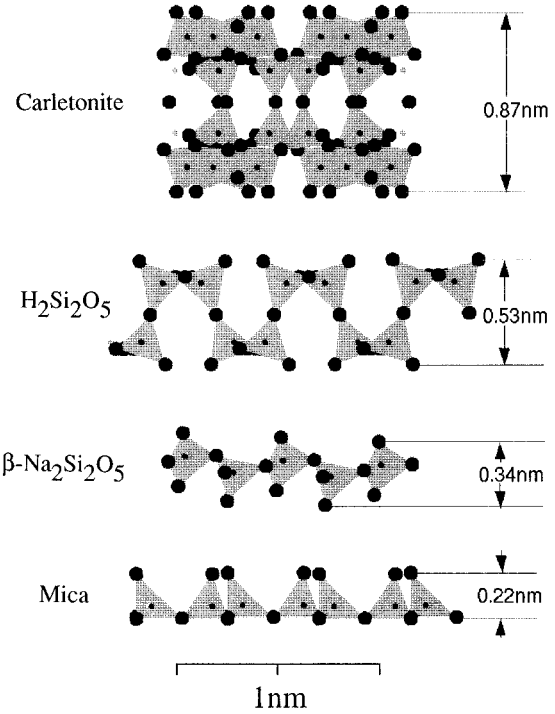

Figure 11. SiO_4 tetrahedral layers in some phyllosilicate minerals containing single and double SiO_4 monolayers.

The XRD simulations offer reasonable estimates of pore diameters and wall thicknesses, coincident with those obtained by TEM and nitrogen adsorption. We now discuss the structure of FSM-16 based on the dimensions determined by the XRD simulations.

The pore-wall thicknesses, 0.4−0.9 nm correspond to the thicknesses of single or double SiO_4 tetrahedral layers observed in crystalline layered silicate minerals. Figure 11 shows SiO_4 tetrahedral layers in various phyllosilicates with single and double layers whose structures are well defined. Thicknesses of the tetrahedral layers were defined as distances between the external oxygen atoms whose atomic positions were determined by using their crystallographic data and denoted in Figure 11. Crystals of $H_2Si_2O_5$,[15] β-$Na_2Si_2O_5$,[16] and mica[17] have single SiO_4 tetrahedral layers with six-membered rings similar to kanemite. The precise crystal structure of kanemite has not yet been determined. Single silicate layers are between 0.22 and 0.53 nm thick, the variation is largely due to different degrees of wrinkling of the tetrahedral layers. The tetrahedral layers in $H_2Si_2O_5$ are very strongly wrinkled, and in β-$Na_2Si_2O_5$ they are slightly less wrinkled and in mica not wrinkled. The double silicate layer in carletonite[18] has a thickness of 0.87 nm.

The pore-wall thickness, 0.4 nm of the as-synthesized sample (HDTMA/FSM-16) may correspond to that of the slightly less wrinkled single silicate layers observed in β-$Na_2Si_2O_5$ (0.34 nm). The surfactant-leached samples, formed by exchange for H^+ (H/FSM-16) and calcination (FSM-16), have almost same wall thicknesses, 0.9 and 0.8 nm, which may correspond to a double silicate layer. The reason the internal structure of kanemite sheet was

(15) Liebau, F. *Z. Kristallogr.* **1964**, *120*, 427−449.
(16) Pant, A. K. *Acta Crystallogr.* **1968**, *B24*, 1077−83.
(17) Wyckoff, R. W. G. *Crystal Structure*; Interscience Publishers: New York, Vol. III, Chapter XII, pp 55−56.
(18) Chao, G. Y. *Am. Mineral.* **1972**, *57*, 765−778.

not retained in the as-synthesized sample (HDTMA/FSM-16) remains open for further study, including the possibility of a continuous "rhombohedral" deformation of a cubic minimum surface as discussed by Dr. S. Hyde.[19]

Most of the increase in the pore wall thickness and decrease in the pore diameter during removal of surfactants could be explained by wrinkling of the silicate layers. Liebau[20] pointed out the relationship between the degree of wrinkling of the tetrahedral sheets and the size of the cation attached to the silicate layers in the phyllosilicate minerals. The degree of the wrinkling is higher for the SiO_4 sheets with smaller cations such as H^+ and Li^+ than that for the SiO_4 sheets with larger cation such as Na^+ as shown in Figure 11. HDTMA/FSM-16 is accordingly expected to have stretched silicate walls, due to the relatively large surfactant cations attached to the silicate walls. In constant H/FSM-16 and FSM-16 have strongly wrinkled silicate walls, due to the smaller H^+ cations attached to the silicate walls. The strongly wrinkled silicate layer has a structure similar to a double silicate layer, as shown in Figure 11. The same O^4/O^3 ratio in ^{29}Si MAS NMR spectra between HDTMA/FSM-16 and H/FSM-16 indicates that the wall thickening is caused by the wrinkling of the silicate wall without condensation. Chen et al.[5] also measured ^{29}Si MAS NMR spectra of MCM-41 materials during removal of surfactants by treating with HCl/ethanol solution. They reported that the Q^4/Q^3 ratio of SiO_4 in the material increased during treatment. This indicates a distinguishing feature of the FSM-16 from the MCM-41 materials. During calcination, condensation of SiO_4 units occurred in the wrinkled silicate layers, which was also observed in ^{29}Si MAS NMR. The smaller pore diameter for FSM-16 than H/FSM-16 is attributable to the higher degree of condensation of the SiO_4 units in the pore wall. The condensation did not affect the pore-wall thickness between H/FSM-16 and FSM-16. However, the wrinkling of silicate sheets cannot explain all of the change in wall thickness from 0.4 to 0.8−0.9 nm. As another possibility, deposition of dissolved silicate species on the pore wall should be considered to thicken the pore walls during removal surfactants. Such dissolved silicate species were formed from kanemite during the synthesis and remained in the as-synthesized FSM-16 material.

Two of the authors have proposed a folded sheets mechanism (FSM) for the formation of FSM-16 materials.[4,21] The formation mechanism leads to a structural model of the as-synthesized FSM-16 material such that the pore walls are composed of single and double SiO_4 layers. The double layers in the model are formed by bonding of the adjacent single layers of kanemite. To date however, we have not succeeded in observing traces of the expected orthorhombic symmetry, due to differences of the wall thicknesses between the single and double monolayers of the as-synthesized FSM-16 material. The pore walls of MCM-41 have been considered to be composed of double SiO_4 monolayers. The MCM-41 model gives the pore wall thickness of ~0.9 nm. It is close to the wall thicknesses (0.8, 0.9 nm) experimentally obtained for FSM-16 and H/FSM-16 but obviously larger than that (0.4 nm) obtained for HDTMA/FSM-16. As far as we know, there are no reports of thickening of pore walls in MCM-41 materials during removal of surfactants. The thin-wall structure of as-synthesized FSM-16 is supported by the unstable nature of the H/FSM-16 structure under water vapor at 25 °C, and the stable silicate framework of FSM-16 is formed during calcination.

Conclusion

The XRD observations together with some simulations furnish reasonable pore diameters and wall thicknesses of the FSM-16 materials which were in agreement with those obtained by TEM and nitrogen adsorption. The as-synthesized FSM-16 material contains thin pore walls of 0.4 nm thick, which may correspond to slightly less wrinkled single SiO_4 layers and an apparent pore diameter of 4.2 nm. The surfactant removed FSM-16 materials had thicker pore walls of 0.8 and 0.9 nm, which may correspond to double SiO_4 layers and pore diameters of 3.4 and 3.7 nm.

Acknowledgment. The authors would like to acknowledge Dr. S. Hyde (the Australian National University) for comment and Mr. N. Suzuki (Toyota Central R&D Labs.) for the TEM observations. O.T. thanks financial support from Ministry of Education, Science and Culture, Japan.

CM960115V

(19) Hyde, S., private communication.
(20) Liebau, F. *Structural Chemistry of Silicates*; Springer-Verlag: Berlin, 1985; pp 198−205.
(21) Inagaki, S.; Fukushima, Y.; Kuroda, K. *In Zeolite and Related Microporous Materials: State of the Art 1994*; Weitkamp, J., Karge, H. G., Pfeifer, H., Holderich, W., Eds.; Elsevier: Amsterdam, 1994; pp 125−132.